Bulgarian Chemical Communications, Volume 50, Special issue H (pp. 74– 79) 2018

Hexane and toluene oxidation on $LaCoO_3$ and $YCoO_3$ perovskite catalysts

M. Markova-Velichkova*, Ts. Lazarova, G. Ivanov, A. Naydenov, D. Kovacheva

Institute of General and Inorganic Chemistry, Bulgarian Academy of Sciences, 1113 Sofia, Bulgaria

Received: January 18, 2018; Revised: March 02, 2018

Solution combustion technique was applied to prepare perovskite-type $LaCoO_3$ and $YCoO_3$ catalysts supported on α-Al_2O_3. X-ray diffraction and scanning electron microscopy were used for physicochemical and morphological characterisation of fresh and worked catalysts. Sample catalytic activity was studied with respect to complete oxidation of hydrocarbons (*n*-hexane and toluene). It was found that *n*-hexane is difficult to oxidise as compared to toluene. Reaction kinetics tests and experiments on so-called 'depletive' oxidation were conducted to establish reaction mechanism. Experimental results showed that Eley-Rideal and Mars-van Krevelen mechanisms were unlikely. The methods applied indicated that toluene complete oxidation on both catalysts proceeded *via* Langmuir-Hinshelwood mechanism by dissociative adsorption of oxygen, the reacting hydrocarbon and oxygen being adsorbed on different active sites. The result proved that lanthanum-containing samples exhibited a higher activity than yttrium catalysts. Different A-positioned cations of perovskite catalysts are discussed about their effect on structural, morphological, and catalytic properties.

Key words: perovskite catalyst, combustion synthesis, hydrocarbon oxidation.

INTRODUCTION

Perovskite-type oxides have been extensively studied over the last decades in terms of their application as catalysts in reactions of hydrocarbon oxidation. They possess some advantages such as low cost, stability at high temperature, and excellent catalytic activity [1–3]. Perovskites have been tested as catalysts for CO oxidation, oxidation of methane to syngas, oxidation of volatile organic compounds and CO + NO reactions [4–6]. Perovskite type oxides have general formula ABO_3. The structure is named after the naturally occurring mineral perovskite ($CaTiO_3$) and is usually described in pseudocubic form. This type of structure offers two positions for the cations. The cation with a large ionic radius (usually rare-earth or alkali-earth metal) occupies A site, while a cation with a smaller ionic radius (for example 3-d transition metal) occupies B site. The number of potentially interesting perovskites in the oxidation reactions is very great owing to the number of A and B cations that can be accomodated into this structure. Lattice distortion magnitude depends on the kind of A cations. In all cobalt-containing perovskites, the cobalt ion is surrounded by weakly distorted oxygen CoO_6 octahedra, whereas the rare-earth ions are situated in distorted cubo-octahedra formed of 12 oxygen ions. The coordination of A cation comprises 12 Ln-O bonds, three of them are long bonds, six are medium-length bonds, and the rest three are short bonds. Cell volume change follows lanthanide contraction. It is well established that on decreasing ionic radius of A cation the perovskite changes from higher to lower symmetry like from cubic to orthorhombic. An increasing rotation of the CoO_6 octahedra with decreasing A ionic radius reduces the Co-O-Co bond angles from 180° in ideal cubic perovskite to 164–146° in almost all $LnCoO_3$. On the other hand, the Co-O bond remains almost constant except for Ln = La with a broad maximum for lanthanide ionic radius about 1.1 Å. The crystal structure of $LaCoO_3$ is different from all other members of the $LnCoO_3$ series. At room temperature, $LaCoO_3$ has a rhombohedrally distorted cubic perovskite structure with unit cell belonging to the space group R-3c and two formulas per unit cell. Replacement of La^{3+} ion of smaller ionic radius by La^{3+} induces a chemical pressure on the CoO_3 array that allows cooperative rotations of CoO_6 octahedra, which relieve the compressive stress on the Co-O bond. Consequently, the Co-O bond length changes a little with ionic size [7]. The structure of $LnCoO_3$ perovskites is very sensitive to temperature changes. Structural distortion magnitude changes significantly with changes in temperature. Evolution of the structure of perovskite rare-earth cobaltites versus temperature governs their magnetic, catalytic, and transport properties. A neutron diffraction study of $LaCoO_3$ versus temperature [8] has shown that there is no deviation from the R-3c symmetry, but the bond lengths exhibit significant anomalies. Many synthesis procedures have been developed in order to produce perovskite mixed oxides of high specific surface area, namely

* To whom all correspondence should be sent
E-mail: markova@svr.igic.bas.bg

co-precipitation [9], citrate complexation [10], spray drying [11], freeze drying [12], flame hydrolysis [13], etc. As an alternative to the above-mentioned methods, solution combustion synthesis offers several attractive advantages such as short time to obtain final product, simplicity of laboratory procedures, high degree of homogeneity of the final product of small crystallite size, cheapness due to energy saving. Solution combustion synthesis has a special advantage of simultaneous synthesis of the desired ceramic phase and its adhesion to the support. In this work, solution combustion technique was applied to prepare perovskite-type $LaCoO_3$ and $YCoO_3$catalysts supported on α-Al_2O_3. Catalytic activity measurements were performed in the reactions of complete oxidation *n*-hexane and toluene.

EXPERIMENTAL

Sucrose-assisted solution combustion method was applied to prepare $LaCoO_3$ and $YCoO_3$ catalysts [14,15]. La_2O_3 (Fluka) or Y_2O_3 (Merck) and $Co(NO_3)_2.6H_2O$ (Merck) were used as initial compounds. Stoichiometric amounts of matching oxide and cobalt nitrate were dissolved in distilled water. The rare-earth oxides were transformed into nitrate form by addition of certain amount of nitric acid. According to described method the nitrate solutions were further mixed with aqueous solution of sucrose at an oxidizing to reducing power ratio of corresponding nitrate and organic fuel of 1:1 [14,15]. The solutions were placed on a heating plate until evaporation of the water. After that, a foamy mass was formed, which burnt to produce an amorphous powder oxide material. As-prepared materials were thermally treated at 400 °C for 1 h in air. Then, the materials were ground for homogeneity. The final synthesis procedure included heat treatment of the catalysts in air at 700 °C for 1 h. At this temperature, the $LaCoO_3$ sample was a single phase, while $YCoO_3$ showed some residual Y_2O_3. Single phase $YCoO_3$ was obtained after additional grinding and heat treatment at 800 °C for 1 h. After the synthesis, a ball milling in a planetary mill for 1 h in isopropanol was applied to both perovskite samples. Spherical pellets of α-Al_2O_3 (with average diameter of 0.9 mm and negligible specific surface area) were used as support. The carrier was dipped into the suspension of perovskite phase and isopropanol. After dipping, the catalysts were dried at 100 °C and heated at 700 °C for 30 min. As a result, the active phase is regularly distributed on the external spherical surface of the support. Powder X-ray diffraction was used at every stage of perovskite phase preparation as well as after deposition on the carrier and catalytic tests. Powder diffraction pat-terns were taken at room temperature on a Bruker D8 Advance diffractometer using CuK_α radiation and LynxEye detector. Measurement range was 10° to 80° 2θ with a step of 0.04° 2θ. XRD data were evaluated by means of EVA and TOPAS 4.2 program packages. SEM photographs of perovskite catalysts were made on a JEOL-JSM-6390 scanning electron microscope.

The catalytic measurements were carried out in a flow type reactor at atmospheric pressure. The test conditions (catalyst volume of 1.0 cm^3, α-alumina spherical particles, fraction of 0.9 ± 0.1 mm, reactor diameter of 10.0 mm, quartz-glass, GHSV of 30000 h^{-1}) were selected after preliminary experiments by applying GHSV from 15000 h^{-1} to 40000 h^{-1}. The measurements were compensated for adiabatic effect by keeping the reaction temperature measured at inlet and outlet of the catalyst bed within ±1 °C. Pressure drop was measured to be below 0.2 m water and was not taken into account. Therefore, the geometrical characteristics of the catalytic reactor permitted to consider it close to isothermal plug flow reactor. The inlet concentrations of reactants were varied as follows: hexane and toluene 115–715 ppm; oxygen 2–21 vol.%; all gas mixtures were balanced to 100% with nitrogen (4.0) and no additional water vapour was added to the gas mixtures. Experiments on so-called 'depletive' oxidation [16] were performed under the same conditions as for the kinetics tests. The nitrogen used for this experiment was of 99.99% purity. Gas analysis was carried out by on-line analysers of $CO/CO_2/O_2$ (Maihak) and THC (total hydrocarbon content, Horiba). A possible formation of organic by-products was monitored by model AL7890A GC-MS apparatus.

RESULTS AND DISCUSSION

Figures 1 and 2 present XRD powder patterns of two catalysts before and after catalytic tests. X-ray data on synthesized perovskites show that the active material is single phase without impurities. $LaCoO_3$ and $YCoO_3$perovskites crystallize in rhombohedral R-3c space group, and orthorhombic Pnma space groups, respectively. The unit cell parameters of perovskite phases have values which are close to the literature data [ICDD PDF-2 (2009) Card No: $LaCoO_3$ – 48-0123, $YCoO_3$ – 75-7970]. Average crystallite sizes of as deposited catalysts were determined by TOPAS 4.2 program and are 63(3) and 88(4) nm for $LaCoO_3$ and $YCoO_3$, respectively (Figs. 1a, 2a). The results can be explained by different synthesis conditions needed to produce single-

phase perovskite materials. Powder XRD patterns of the catalysts manifested also diffraction peaks of the α-Al_2O_3 carrier. Rietveld quantification applied to the powder diffraction patterns revealed that active phase amount was 1.5 and 4.8 (±0.4) mass% for $LaCoO_3$ and $YCoO_3$, respectively (Figs. 1b, 2b). After catalytic tests a slight narrowing of the diffraction peaks was observed, which can be associated with increased crystallite size of the working catalysts (Figs. 1c, 2c).

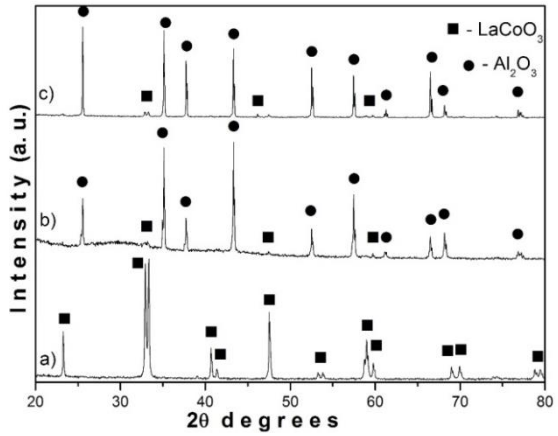

Fig. 1. XRD patterns of: a) initial $LaCoO_3$ perovskite, b) $LaCoO_3$ deposited on α-Al_2O_3, and c) $LaCoO_3$/α-Al_2O_3 catalytic tests.

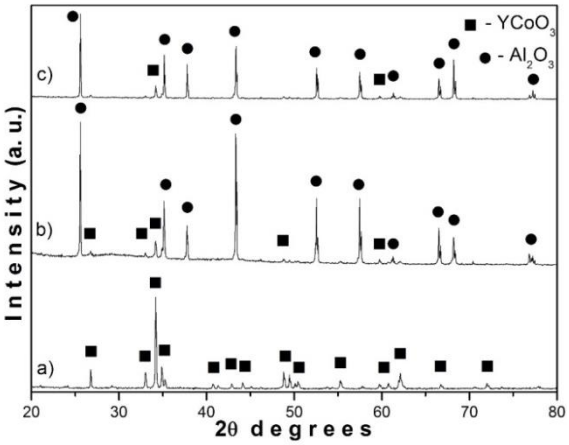

Fig. 2. XRD patterns of: a) initial $YCoO_3$ perovskite, b) $YCoO_3$ deposited on α-Al_2O_3, and c) $YCoO_3$/α-Al_2O_3 catalytic tests.

SEM images of different magnification of as-prepared catalysts are shown in figure 3. It is seen that deposition technique leads to uniform distribution of perovskite phase onto the surface of the carrier. Photographs of higher magnification revealed catalyst microstructure. Particles of the active phase at the surface are about 1–3 μm in size and many pores exist in the interstice among them. The specific surface area of both samples is about 10–15 m^2/g. A difference in particle morphology is also seen. For La sample, the shape of the particles is predominantly plate-like, while the Y sample exposes aggregates of small grain-like particles.

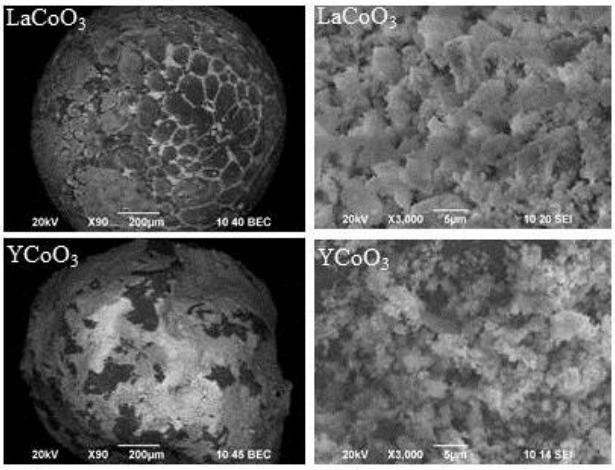

Fig. 3 SEM images of different magnification of the Al_2O_3-supported perovskite catalysts.

Results from catalytic activity measurements of complete oxidation of toluene and *n*-hexane are displayed in figures 4–6. Obviously, the activities of the two catalyst samples are very different, $LaCoO_3$ being more active than $YFeO_3$. An explanation for the significant difference in catalytic activity between $LaCoO_3$ and $YCoO_3$ should be found in structural peculiarities due to the presence of different A cations and their influence on perovskite phase stability and catalytic activity. In the present study difference between the two perovskite structures originates mainly from difference in A cation size, being 1.36 Å for La^{3+} and 1.075 Å for Y^{3+} of the same coordination. For comparison, the ionic radius of O^{2-} is 1.35 Å. Several factors have been proposed to evaluate the stability of the perovskite structures [17,18]. Based on crystal structure data on $LaCoO_3$ and $YCoO_3$, calculated tolerance factor, being equal to 1 for ideal perovskite structure, is 1.0112 for $LaCoO_3$ and 0.9049 for $YCoO_3$. As it can be seen the Y-containing perovskite has more deformed structure and smaller tolerance factor than the La-containing counterpart has. This means that the Y-containing structure is more unstable towards external mechanical, thermal, or chemical influence [19]. $LaCoO_3$ structure stability indicates that this oxide can easily accommodate certain amount of cation and anion defects without structural changes. It is well known that this compound can be synthesized with some deviation from stoichiometry [20]. Previous studies [21] revealed a clear distinction in thermal expansion between $LaCoO_3$ and $YCoO_3$. The Co-O-Co bond angles in $YCoO_3$ decrease with temperature above the onset of spin transition in contrast to $LaCoO_3$, where the Co-O-Co angles constantly increase with temperature. A more

active catalytic behaviour of $LaCoO_3$ can be explained with less deformed (and less deformable) crystal structure compared to that of $YCoO_3$. The Co-O-Co bond angle of $YCoO_3$ is very small (about 148°) and practically remains stable up to 600 K, followed by a decrease with temperature above the onset of spin transition. This leads to a slightly larger expansion of the CoO_6 octahedra compared to lattice expansion. On the other hand, at room temperature the Co-O-Co bond angle in $LaCoO_3$ is about 164° and monotonically increases with temperature, which results in a slightly smaller expansion of the CoO_6 octahedra with respect to lattice expansion [21]. Such a different behaviour has been attributed to a higher symmetry of the $LaCoO_3$ structure compared to $YCoO_3$ (Pbnm) [19]. Catalytic tests showed that sample activity towards toluene was significantly higher than that with hexane (Fig. 4) and further investigation was concentrated on toluene combustion.

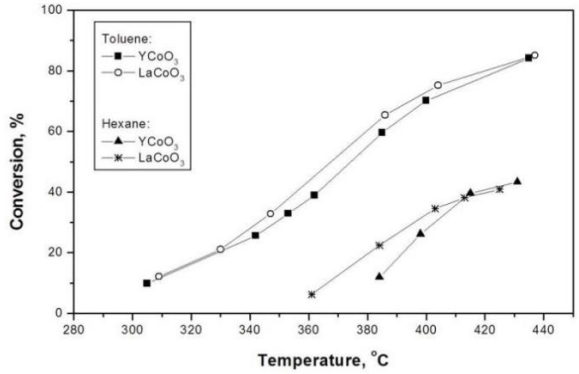

Fig. 4. Complete oxidation of toluene and hexane in air on alumina-supported $YCoO_3$ and $LaCoO_3$: effect of reaction temperature on hydrocarbon conversion degree.

For calculation of kinetics parameters, inlet concentrations of both hydrocarbon and oxygen reactants were varied. Concentration dependence on conversion leads to the conclusion that first order kinetics should be excluded. An Eley-Rideal mechanism should not be considered since the reaction is not first order in oxygen. Regarding Mars-van Krevelen mechanism (oxi-redox) bulk oxygen from the active phase must take part in the reaction. In order to find out which mechanism is more probable, experiments on so-called 'depletive' oxidation were performed [16]. The latter involve measurements of the formation of oxidation products (CO and CO_2) when oxygen supply to the gas mixture is stopped after achieving stationary conditions at a temperature for 33% conversion. The reason for these experiments is to find out whether oxygen from the catalyst participates in the oxidation process. Results from the 'depletive' oxidation are presented in figure 5.

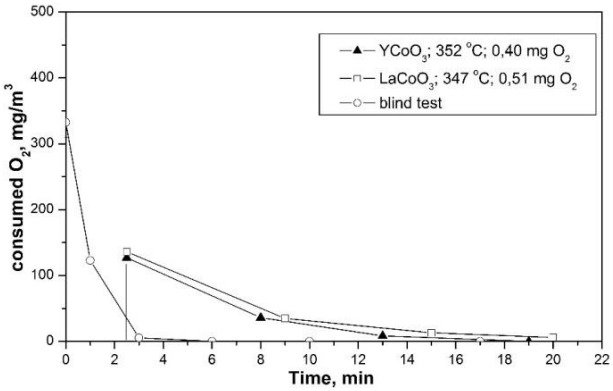

Fig. 5. 'Depletive' oxidation at temperatures for 33% conversion of toluene.

Following termination of the oxygen supply to the gas feed, formed amount of $CO+CO_2$ in each test was calculated from the area under the transient curves. The surface or lattice oxygen, which takes part in the reaction, was estimated based on formed $CO+CO_2$ quantities during 'depletive' oxidation, experiment duration being 20 min. Very small amounts of surface or lattice oxygen (0.3–0.5 mg, below 1.5% of active phase) and the absence of phase transformations after the catalytic tests reveal that bulk oxygen from the active phase is not involved in the reaction, i.e. the Mars-van Krevelen mechanism should not be considered likely. Finally, power law kinetics (PWL) and four mechanistic models (Langmuir-Hinshelwood, bimolecular reaction, surface reaction being the rate-determining step) were fitted with the experimental data. Fitting of the kinetics parameters was performed applying of an integrated computer program for simultaneous solution of the material balance in isothermal plug flow reactor and numerical nonlinear optimization procedure based on iterative gradient reduction. For finding a global minimum, residuals squared sum (RSS) between experimental data and model predictions was minimized upon starting from several different initial values of the varying parameters. As an additional measure, the absence of trends in the RSS distribution was controlled and the square of correlation coefficient (R^2) was calculated.

Two Langmuir-Hinshelwood models assume that the hydrocarbon and the oxygen are adsorbed on different sites and oxygen adsorption is non-dissociative (LH-DS-ND) or dissociative (LH-DS-D). Other two LH models suppose competitive adsorption of hydrocarbon and oxygen on one-type sites and non-dissociative (LH-OS-ND) or dissociative (LH-OS-D) adsorption of oxygen. Kinetics parameters are given in Table 1.

Table 1. Reaction rate expressions and kinetics parameters for applied power law and Langmuir-Hinshelwood models

PWL $r = kP_{voc}^{m}P_{ox}^{n}$	Catalyst	k_o	E_a	m	n			RSS	R^2
	$YCoO_3$	1.35E+06	75 656	0.29	0.33			2.05	0.99
	$LaCoO_3$	2.36E+06	78 260	0.31	0.19			1.79	0.99
LH-DS-ND $r = \frac{kK_{voc}K_{ox}P_{voc}P_{ox}}{(1+K_{voc}P_{voc})(1+K_{ox}P_{ox})}$	Catalyst	k_o	E_a	$k_{o,voc}$	ΔH_{voc}	$k_{o,ox}$	ΔH_{ox}	RSS	R^2
	$YCoO_3$	5.41E+06	93720	2.71E-03	-60644	2.40E+01	-1269	3.77	0.975
	$LaCoO_3$	2.74E+07	101219	7.95E-05	-77677	2.80E+02	*+7396*	1.12	0.992
LH-DS-D $r = \frac{kK_{voc}P_{voc}K_{ox}^{1/2}P^{1/2}}{(1+K_{voc}P_{voc})(1+K_{ox}^{1/2}P_{ox}^{1/2})}$	Catalyst	k_o	E_a	$k_{o,voc}$	ΔH_{voc}	$k_{o,ox}$	ΔH_{ox}	RSS	R^2
	$YCoO_3$	3.80E+07	99839	4.21E-04	-70751	1.03E-01	-15724	2.22	0.985
	$LaCoO_3$	6.46E+07	104294	4.72E-05	-80584	1.12E+00	-16995	0.75	0.995
LH-OS-ND $r = \frac{kK_{voc}K_{ox}P_{voc}P_{ox}}{(1+K_{voc}P_{voc}+K_{ox}P_{ox})^2}$	Catalyst	k_o	E_a	$k_{o,voc}$	ΔH_{voc}	$k_{o,ox}$	ΔH_{ox}	RSS	R^2
	$YCoO_3$	5.06E+07	97888	9.44E-03	-51410	1.87E-03	-45118	6.52	0.960
	$LaCoO_3$	7.56E+06	87572	4.08E-02	-45523	1.71E-05	-73715	4.65	0.967
LH-OS-D $r = \frac{kK_{voc}K_{ox}^{1/2}P_{voc}P_{ox}^{1/2}}{(1+K_{voc}P_{voc}+K_{ox}^{1/2}P_{ox}^{1/2})^2}$		k_o	E_a	$k_{o,voc}$	ΔH_{voc}	$k_{o,ox}$	ΔH_{ox}	RSS	R^2
	$YCoO_3$	2.27E+08	101208	3.87E-03	-52372	6.30E-04	-37006	2.41	0.984
	$LaCoO_3$	9.49E+07	99285	4.37E-04	-65667	1.97E-01	-20287	1.01	0.993

E_{ai}, J/mol; ΔH_i, J/mol; k_{oi}, atm^{-1}; $k = k_o . \exp(-E_a/RT)$; $K_i = k_{o,(voc,ox)} . \exp(-\Delta H_{i,voc,ox}/RT)$; $\Delta H_i = E_{ad} - E_{des}$)

Figure 6 displays model consistency as a difference between standard measurement error of conversion and RSS.

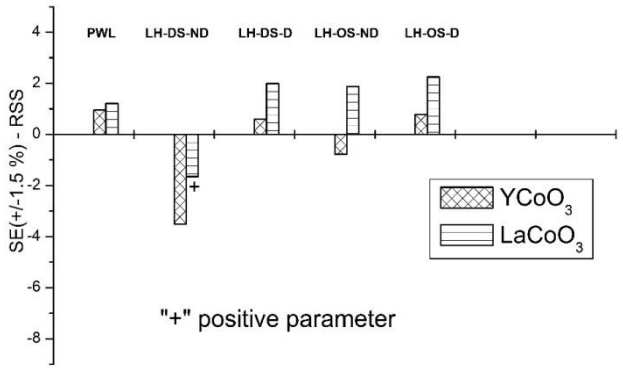

Fig. 6. Consistency of model prediction with catalytic test errors.

Evidently, four of the models (PWL, LH-DS-ND, LH-DS-D, LH-OS-D) are consistent with measurement confidence interval, while LH-OS-ND should be considered non-satisfactory. In addition, the latter model suggests non-dissociative adsorption of the oxygen. With one of the models (LH-DS-ND and $LaCoO_3$) the obtained value for ΔH of the oxygen adsorption is positive, which has no physical sense and is a reason to reject this model. It is obvious that a fit that is more adequate was obtained with the models which predict dissociative adsorption of oxygen. Among considered Langmuir-Hinshelwood models, the values for RSS with LH-DS-D are the lowest, which can be taken as supplementing information to conclude that the hydrocarbons and oxygen are adsorbed on different sites and oxygen adsorption is dissociative.

CONCLUSIONS

Two perovskite-type catalysts ($LaCoO_3$ and $YCoO_3$, supported on α-Al_2O_3 spherical particles) were synthesized *via* sucrose-assisted solution combustion method. Mean crystallite size varied between 63(3) nm for $LaCoO_3$ and 88(4) nm for $YCoO_3$. Catalytic activity measurements with respect to complete oxidation of hydrocarbons (*n*-hexane and toluene) showed that aliphatic hydrocarbon was found to be difficult to oxidize, while with aromatic compound (toluene) a promising activity was observed. $LaCoO_3$ more active catalytic behaviour of could be explained by less deformed (and less

deformable) crystal structure compared to $YCoO_3$. It can be concluded that the reaction of complete oxidation of toluene on perovskite-type catalysts ($LaCoO_3$ and $YCoO_3$, supported on α-Al_2O_3) proceeds *via* Langmuir-Hinshelwood mechanism with dissociative adsorption of oxygen, the reacting hydrocarbon and oxygen being adsorbed on different sites.

***Acknowledgement**: This work was performed with financial support through collaborative project between Bulgarian Academy of Sciences and Macedonian Academy of Sciences and Arts 'Structural characterisation and investigation of the electrical and catalytic properties of newly synthesised inorganic and organic-inorganic perovskites'.*

REFERENCES

1. R. Zhang, H. Alamdari, S. Kaliaguine, *Appl. Catal. B: Environ.*, **72**, 331 (2007).
2. M. Natile, E. Ugel, C. Maccato, A. Glisenti, *Appl. Catal. B: Environ*., **72,** 351 (2007).
3. S. Hosseini, M. Sadeghi, A. Alemi, A. Niaei, D. Salari, L. Kafi-Ahmadi, *Chin. J. Catal*., **31**, 747 (2010).
4. E. Arenolt, A. Maione, A. Klisinska, A. Sanz, M. Montes, S. Shares, J. Blanco, *Appl. Catal. A: General*, **339**, 1 (2008).
5. G. Pecchi, P. Reyes, R. Zamora, C. Campos, L. Cadus, B. Barbero, *Catal. Today*, **133-135**, 420 (2008).
6. J. Dacquin, C. Lancelot, C. Dujardin, P. Da Costa, G. Djega-Mariadassou, P. Beaunier, S. Kaliaguine, S. Vaudreuil, S. Royer, P. Granger, *Appl. Catal. B: Environ*., **91**, 596 (2009).
7. J.-S. Zhou, J.-Q. Yan, J. B. Goodenough, *Phys. Rev. B*, **71**, 220103(R), (2005).
8. G. Maris, Y. Ren, V. Volotchaev, C. Zobel, T. Lorenz, T. T. M. Palstra, *Phys. Rev. B*, **67**, 224423 (2003).
9. P. K. Gallagher, *Mater. Res. Bull*., **3**, 225, (1967).
10. H.-M. Zhang, Y. Teraoka, N. Yamazoe, *Chem. Lett*., 665 (1987).
11. R. J. H. Voorhoeve, D. W. Johnson, J. P. Remeika, P. K. Gallagher, *Science*, **195**, 827 (1977).
12. J. Kirchnerova, D. Klvana, *Int. J. Hydrogen Energy*, **19,** 501 (1994).
13. R. A. M. Giacommuzi, M. Portinari, I. Rossetti, L. Forni, *Stud. Surf. Sci. Catal*., **130**, 197 (2000).
14. S. Biamino, C. Badini, *J. Eur. Ceram. Soc*., **21**, 3021 (2004).
15. S. Biamino, P. Fino, D. Fino, N. Russo, C. Badini, *Appl. Catal. B: Environ.*, **61**, 297 (2005).
16. C. Brooks, *J. Catal*., **8**, 272 (1967).
17. A. Mineshige, M. Inaba,T. Yao, Z. Ogumi, *J. Solid State Chem*., **121**, 423 (1996).
18. J. E. Sunstrom IV, K. V. Ramanujachary, M. Greenblatt, M. Croft, *J. Solid State Chem*., **139**, 388 (1998).
19. M. James, D. Cassidy, D. J. Goossens, R. L. Withers, *J. Solid State Chem*., **177**, 1886 (2004).
20. J. Mira, J. Rivas, M. Vázquez, J. M. García-Beneytez, J. Arcas, R. D. Sánchez, M. A. Señarís-Rodríguez, *Phys. Rev. B*, **59**, 123 (1999).
21. P. G. Radaelli, S.-W. Cheong, *Phys. Rev. B*, **66**, 094408 (2002).

ОКИСЛЕНИЕ НА ХЕКСАН И ТОЛУЕН ВЪРХУ $LaCoO_3$ И $YCoO_3$ ПЕРОВСКИТОВИ КАТАЛИЗАТОРИ

М. Маркова-Величкова*, Ц. Лазарова, Г. Иванов, А. Найденов, Д. Ковачева

Институт по обща и неорганична химия, Българска академия на науките, 1113 София, България.

Постъпила на 18 януари 2018 г.; Преработена на 2 март 2018 г.

(Резюме)

Перовскитови $LaCoO_3$ и $YCoO_3$ катализатори бяха синтезирани по метода на изгаряне от разтвор и нанесени на α-$A1_2O_3$ носител. Физикохимично и морфологично охарактеризиране на получените и работили катализатори беше извършено с методите рентгенова дифракция и сканиращата електронна микроскопия. Каталитичната активност е изследвана по отношение на пълното окисление на въглеводороди (хексан и толуен). Установено е, че хексанът се окислява по-трудно в сравнение с толуена. Реакционният механизъм беше изследван с кинетични тестове и чрез опити върху така нареченото „деплетивно" окисление. Получените резултати показват, че механизмите на Ели-Ридиъл и Марс-ван Кревелен не са вероятни, а най-висока степен на предвиждане на опитните резултати се постига при прилагане модела на Лангмюр-Хиншелуд (дисоциативна адсорбция на кислород, реагиращите въглеводород и кислород се адсорбират на различни активни центрове). От сравнителен анализ е установено, че пробата, съдържаща лантан, притежава по-висока активност, отколкото тази, съдържаща итрий. Дискутирана е ролята на различните катиони в А позиция върху структурните, морфологични и каталитични свойства на перовскитовите катализатори.